High-Brightness High-Energy Electron Beams from a Laser Wakefield Accelerator via Energy Chirp Control

W. T. Wang,[1] W. T. Li,[1] J. S. Liu,[1,2,*] Z. J. Zhang,[1] R. Qi,[1] C. H. Yu,[1] J. Q. Liu,[1] M. Fang,[1] Z. Y. Qin,[1]
C. Wang,[1] Y. Xu,[1] F. X. Wu,[1] Y. X. Leng,[1] R. X. Li,[1,2,3,†] and Z. Z. Xu[1,2,3,‡]

[1]*State Key Laboratory of High Field Laser Physics, Shanghai Institute of Optics and Fine Mechanics,
Chinese Academy of Sciences, Shanghai 201800, China*
[2]*Collaborative Innovation Center of IFSA, Shanghai Jiao Tong University, Shanghai 200240, China*
[3]*School of Physical Science and Technology, ShanghaiTech University, Shanghai 200031, China*

By designing a structured gas density profile between the dual-stage gas jets to manipulate electron seeding and energy chirp reversal for compressing the energy spread, we have experimentally produced high-brightness high-energy electron beams from a cascaded laser wakefield accelerator with peak energies in the range of 200–600 MeV, 0.4%–1.2% rms energy spread, 10–80 pC charge, and ~0.2 mrad rms divergence. The maximum six-dimensional brightness $B_{6D,n}$ is estimated as ~6.5×10^{15} A/m^2/0.1%, which is very close to the typical brightness of e beams from state-of-the-art linac drivers. These high-brightness high-energy e beams may lead to the realization of compact monoenergetic gamma-ray and intense coherent x-ray radiation sources.

The past decade has witnessed remarkable progress in the field of electron acceleration based on the laser wakefield accelerator (LWFA) concept [1–4]. The ultrahigh accelerating gradient reaching 100 GV/m makes the LWFA very attractive as a compact accelerator. Quasimonoenergetic e beams at peak energies of multi-GeV have been experimentally generated [5–7]. However, a controllable high-quality e-beam source with desirable all-round properties such as lower energy spread, lower emittance, and larger beam charge at the same time, might not be obtained in a single-staged LWFA, because the electron injection and the electron acceleration are coupled together and thus cannot be controlled independently. Recent experimental endeavors by exploiting the injection scheme with two colliding laser pulses or self-truncated ionization have produced e beams with a few percent energy spread [8,9]. Cascaded acceleration of electrons by decoupling the injection and the acceleration provides an attractive route to control e-beam parameters such as peak energy, energy spread, and beam charge [10–13]. The cascaded LWFAs using ionization-induced injection has shown that the e beam's relative energy spread (RES) can be greatly reduced [10,13]. However, the RES is still at the several-percent level.

In this Letter, we experimentally demonstrate a new scheme of the cascaded LWFA via manipulating electron injection, quasi-phase-stable acceleration, electron seeding in different periods of the wakefield, as well as controlling energy chirp reversal for realizing energy spread compression. High-quality e beams with energies in the range of 200–600 MeV, 0.4%–1.2% rms energy spread, 10–80 pC charge, and ~0.2 mrad rms divergence are experimentally obtained in this new cascaded acceleration scheme. The

maximum 6D brightness $B_{6D,n}$ which is defined as the peak current in the e-beam core divided by the product of the rms transverse normalized emittances and the fractional energy spread rms in units of 0.1% [14], is estimated as ~6.5×10^{15} A/m^2/0.1%, which is about 5 times of that previously reported from a LWFA [15,16]. The all-round properties of e beams achieved here are most likely to meet the requirement for realizing a high-gain soft x-ray free-electron laser if using a transverse gradient undulator [17]. Three-dimensional particle-in-cell (3D PIC) simulations support this attractive cascaded LWFA scheme for generating controllable high-quality e beams.

Figure 1(a) shows the schematic of the experimental setup for producing high-quality e beams via cascaded acceleration in the gas flow with a structured density profile. The experiments were carried out at the laser facility with 30-fs pulse duration, 200-TW peak power, and 1-Hz repetition rate based on the chirped pulse amplification using Ti:sapphire [18]. The 33-fs, 800-nm laser pulses with an on-target power of 100–120 TW were focused by a $f/30$ off-axis parabolic mirror onto the gas target and the vacuum beam radius ω_0 was measured to be 32 μm full width at half maximum (FWHM). The fractional laser energy contained within the laser spot was measured to be ~61.4% at $1/e^2$, and the peak intensity was estimated to be 3.6–4.3×10^{18} W/cm^2 corresponding to a normalized amplitude of $a_0 \approx 1.3$. In these focal spot measurements, a tiny part of the laser energy was used in order to avoid self-phase modulation or filamentation. The gas target was manipulated by two pulsed gas valves connected to two nozzles with different bore diameters, respectively. The first nozzle diameter was 800 μm, and the
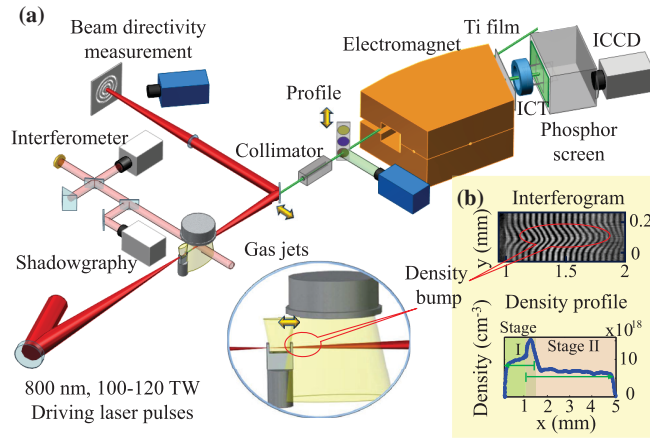
FIG. 1.   (a) Experimental layout of the cascaded LWFA using two gas jets. (b) The measured plasma density profile with a "density bump" between the two-segment plasmas.

FIG. 2.   Measured e-beam energy spectra and 6D brightness $B_{6D,n}$. (a) Angle-resolved energy spectra of a series of high-quality e beams with peak energies in the range of 530–580 MeV. (b) Angle integrated energy spectra of the e beams corresponding to (a). (c) The statistic 6D brightness $B_{6D,n}$ of the e beams corresponding to (a).

second one was 4 mm. By adjusting the horizontal span between two gas nozzles, a structured gas profile with a steep density bump between two-segment gases can be produced. The right wall of the first gas nozzle which was inserted in the downstream of the second supersonic flow was acting as an obstacle to generate this density bump. A probe beam split from the main laser beam was sent perpendicularly across the gas jet, then entered a Michelson-type interferometer using a $4f$ optical imaging system for measuring the plasma density. As shown in Fig. 1(b), an interferogram and the retrieved plasma density profile indicated a density bump region with a scale of ~250 μm.

The laser-accelerated e beams were deflected by a 90-cm-long tunable dipole electromagnet with a maximum magnetic field of 1.1 T, and measured by a Lanex phosphor screen imaged onto an intensified charge-coupled device (ICCD) camera in a single shot, which was cross calibrated by using a calibrated imaging plate and an integrating current transformer (ICT) to measure the charge of the e beams [19]. The uncertainty of the measured e-beam charge was estimated to be within ±12%. The energy spectrometer had an energy resolution of 0.2% at 500 MeV with 0.1 mrad divergence, and the uncertainty of the measured peak energy was calculated as ±2% considering the e-beam's pointing uncertainty of ±1 mrad.

In the experiments, the first-segment 0.8-mm-thick gas flow using pure He atoms was operated with a high plasma density of $(1.1 \pm 0.1) \times 10^{19}$ cm^{-3} and the second-segment 4-mm-thick gas flow with an average density of $(6.0 \pm 0.5) \times 10^{18}$ cm^{-3}. As shown in Fig. 1(b), the measurements from the interferometer indicated there was a rapid increase in the density profile (density bump) from 1 to 1.25 mm at ~200 μm away from the exit of the first gas nozzle. Figure 2 shows the measured two-dimensional energy spectra of e beams while firing the 110-TW laser pulses into the gas target. Also shown are the spatially
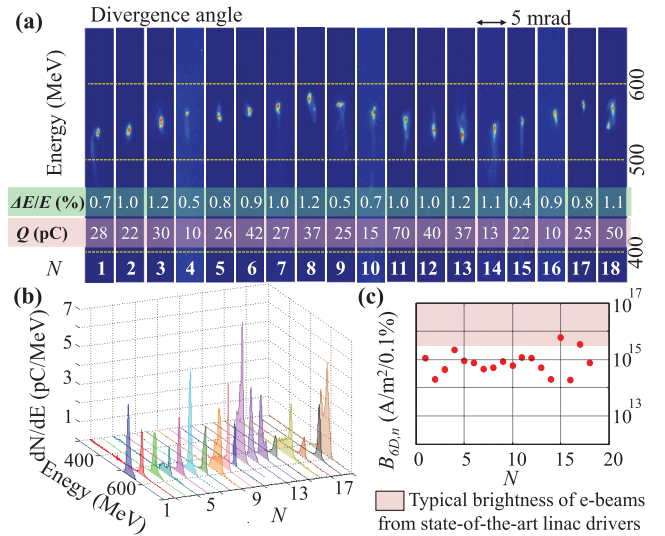
integrated energy spectra and the statistic 6D brightness $B_{6D,n}$ of the e beams. Stable low-energy-spread e beams with peak energies (E) in the range of 530–580 MeV were produced with an energy fluctuation of ±5%. The rms energy spread ($\Delta E/E$) of the produced e beams were mostly scattered within 1% and the rms divergence were around 0.2 mrad. The beam charge (Q) fluctuated from 10 to 70 pC. The fluctuation in e-beam parameters were mainly attributed to the shot-to-shot fluctuation in laser power within 3% and jitter in gas density. Owing to the high plasma density of $(6.0 \pm 0.5) \times 10^{18}$ cm^{-3} used in the experiments, the obtained e-beam energies beyond 500 MeV exceeded far more than the maximum energy gain (~390 MeV) limited by the dephasing length in a single-stage LWFA at such a high density [20]. Quasi-phase-stable acceleration mechanism, under which the accelerated e beam can be kept at a quasistable phase in a laser-driven wakefield [21–23], was excluded because the descending gas density at the tail was produced in our case. This indicated that it should be a result of cascaded acceleration of electrons in different buckets of the laser-driven wakefield where an effective dephasing length can be much longer than that for a single-stage LWFA [23]. As compared with the shock-front injection where the electron injection was manipulated to occur in the first wake period, the produced e beam could not be extended to higher energy simply via the acceleration in one bucket due to the rapid dephasing [24]. The minimal energy spread of 0.4% and divergence of 0.1 mrad obtained in this work should be the best experimental results ever reported. As shown in Fig. 2(b), the maximum e-beam charge number per MeV
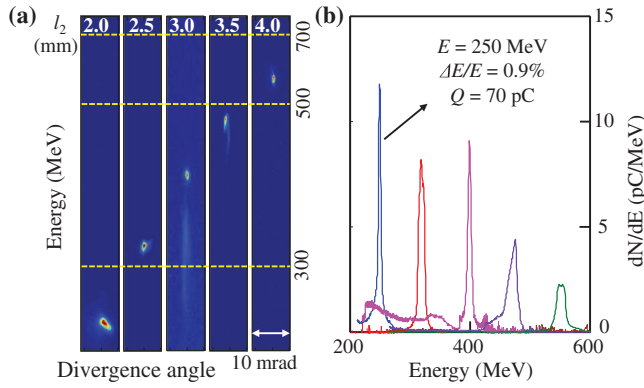
FIG. 3. Measured energy spectra of high-quality e beams while adjusting the length of the second-segment plasma (l_2) from 2.0 to 4.0 mm. Angle resolved (a) and integrated (b) spectra of tunable e beams with peak energies (E) ranging from 250 to 550 MeV, respectively.

remains in the range of 1–7 pC/MeV, which is also the highest value ever reported in this energy range. The 6D brightness $B_{6D,n}$ of the e beams at the exit of the LWFA mostly vibrates around the level of $\sim10^{15}$ A/m^2/0.1%, as shown in Fig. 2(c). In the calculation of $B_{6D,n}$, the transverse normalized emittance is estimated by $\epsilon_n = \gamma\sigma_x\sigma_\theta$, where γ is the relativistic Lorentz factor, σ_x and σ_θ are the transverse size and rms divergence of the e beam, respectively. The e-beam size σ_x and duration at the exit of the LWFA are not measured but are assumed to be 3 μm and 10 fs, respectively, according to the following theoretical simulation results. They are also comparable with the reported values [25–27]. The maximum 6D brightness $B_{6D,n}$ in this work is very close to the typical brightness of e beams from state-of-the-art linac drivers [14] and about 5 times of that previously reported from a LWFA [15,16].

By adjusting the length of the acceleration stage, we obtained monoenegetic e beams with peak energies (E) tunable from 200 to 600 MeV, as shown in Fig. 3. The rms energy spread ($\Delta E/E$) of the produced e beams mostly fluctuated around 1% and the rms divergence were around 0.3 mrad. The little change in the relative energy spread in the range of 200–600 MeV indicated that the increase of absolute energy spread was almost balanced by the increase of the peak energy. The spatially integrated energy spectra [Fig. 3(b)] indicated that a charge per energy interval of more than 10 pC/MeV was reached. The all-round properties of e beams achieved here such as the low energy spread ($\sim$1%), large charge (80 pC), and low divergence (0.26 mrad), are already very close to satisfying the requirements for demonstrating a high-gain soft x-ray free-electron laser if using a transverse gradient undulator [17].

Three-dimensional particle-in-cell simulations using a structured density profile with a density bump between the two-segment plasmas were carried out to explain the cascaded acceleration scheme via different buckets of the laser-driven wakefield. The simulation was performed with

the code VORPAL [28] version 6.2.8 using parameters matching the experimental conditions. The simulation window had three spatial dimensions without periodic boundary conditions. The longitudinal and transverse window sizes were 42 and 136 μm, respectively. The grid cell size was determined as follows: $\triangle x = 0.04$, $\triangle y = \triangle z = 0.2$ μm. A linearly polarized laser pulse with wavelength $\lambda_0 = 0.8$ μm, normalized amplitude $a_0 = 1.2$, pulse duration $\tau = 33$ fs, and FWHM spot size $\omega_0 = 31$ μm, was incident from the left boundary of the simulation box along x. The laser pulse was assumed to be a Gaussian function and the plasma profile was chosen to fit the measured density profile. It began with an upward density ramp followed by a 1-mm-long plateau with the density of 1×10^{19} cm^{-3}, then a density bump with the maximum density of 1.4×10^{19} cm^{-3} and a length of 250 μm, which was followed by a 250 μm downward density ramp and a segment of 1.5-mm-long plasma with the density of 0.6×10^{19} cm^{-3}.

As the laser pulse propagated to $x = 0.90$ mm in the first plateau, the laser intensity a_0 increased rapidly from 1.2 to 6 owing to the intense relativistic self-focusing of the laser beam, as shown in Fig. 4(a). Also shown in Fig. 4(a) was the evolution of the phase velocity β_p, which decreased due to the rapid increase of the laser intensity as described by $\beta_p \approx -4/(ck_p\sqrt{a}) \times da/dt + \beta_\phi$, where k_p is plasma wave number, c denotes the light speed in vacuum, and β_ϕ is the wake phase velocity without accounting for the effect of the pulse intensity evolution [23]. The first self-injection occurred in the second bucket when the laser intensity a increased to 5.0 at $x = 0.78$ mm, owing to the rapid variation of the plasma wave phase velocity β_p, as shown in Fig. 4(a). The laser intensity decreased after $x = 0.90$ mm, and the wake phase velocity increased accordingly. Because a density bump followed at $x = 1$ mm, the β_p increased rapidly and became higher than the light speed in vacuum. Although the laser pulse experienced another intense self-focusing starting from $x = 1.09$ to 1.18 mm and the intensity a increased from 4.5 to 6.8 rapidly, the wake phase velocity β_p could still remain higher than the light speed in vacuum because the density bump could counteract the influence of the rapid increase of the laser intensity. As compared with the two-segment plasmas without the density bump, as shown in Fig. 4(b), the rapid decrease of the wake phase velocity β_p at $x = 1.14$ mm owing to the rapid increase of the laser intensity would induce the second electron self-injection. Therefore, by constructing a density bump between the two-segment plasmas, the second electron injection could be prohibited.

Furthermore, the self-injected electron in the second bucket could be more efficiently accelerated in a quasi-phase-stable way via rephasing in the density bump region where the wake phase velocity β_p was higher than the light speed in vacuum [23,29]. Figures 4(c)–4(f) present 4 typical snapshots of the 2D electron density distribution
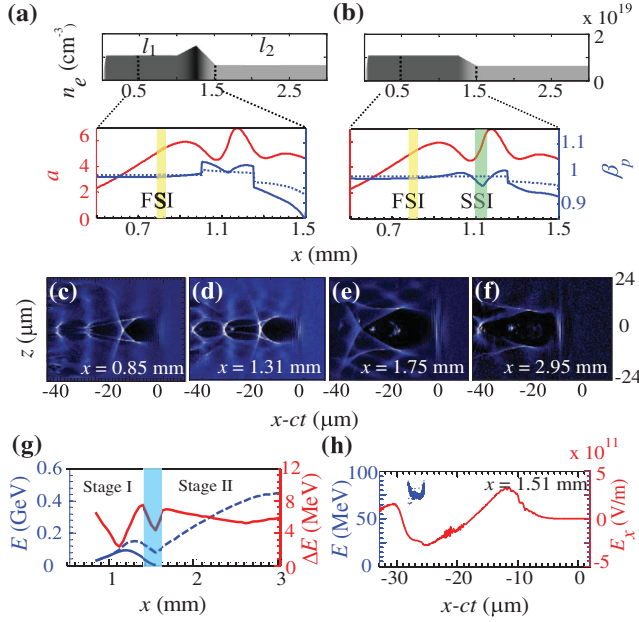
FIG. 4.   Particle-in-cell simulations illustrating the cascaded electron acceleration scheme in different buckets of a laser-driven wakefield. Plasma density profiles applied, evolutions of normalized intensity a (in red) and the corresponding phase velocity β_p of the second bucket (in blue) for the cases with (a) and without the density bump (b), respectively. The dashed blue line corresponds to the variation of the phase velocity caused by the density bump alone. FSI (yellow area) and SSI (green area) show the regions where first self-injection and second self-injection occur, respectively. (c)–(f) The snapshots of electron density distribution in the x-z plane for different x position. (g) Evolutions of the peak energy of the accelerated e beams for the cases with (dashed line in blue) and without the density bump (solid line in blue), respectively. Also shown is the evolution of the absolute energy spread (solid line in red) of the target e beam in the case with the density bump. The light blue area represents the region where the target e beam witnesses a wakefield with a negative slope. (h) Energy distribution of the target e beam along x at $x = 1.51$ mm and the corresponding on-axis wakefield E_x. The e beam is located in the negative-slope region of the wakefield.

for different stages, indicating electron injection and acceleration in the second bucket, and electron seeding and acceleration in the first bucket, respectively. As shown in Fig. 4(g), the injected e beam in the second bucket could be accelerated twice in the two different buckets to the peak energy of 451.3 MeV when the density bump was used. Moreover, it was found that the seed e beam experienced a segment of negative-slope wakefield in the downward density ramp where the energy chirp could be reversed from the positive one to the negative one (high-energy electrons in the front and low-energy electrons at the tail) before being seeded into the first bucket for re-acceleration, as shown in Fig. 4(h). After being seeded into the first bucket for re-acceleration, the low-energy electrons at the tail would gain more energy than the high-energy electrons
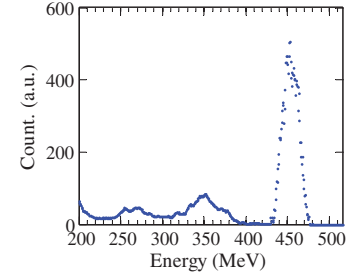

FIG. 5.   Energy spectrum of the generated e beam for the case with the density bump.

in the front owing to the positive-slope wakefield. This is the energy chirp compensation in wakefield acceleration. The absolute energy spread of the e beam would be minimized when the energy chirp was fully compensated. After that, the absolute energy spread would increase. Therefore, by experiencing this energy chirp reversion in the downward density ramp, the growth of the e beam's absolute energy spread could be significantly suppressed owing to the chirp compensation in the re-acceleration as shown in Fig. 4(g). The energy spectrum was shown in Fig. 5, the rms relative energy spread was ~1.4%, and the beam charge was about 66.2 pC, which was quite in agreement with the experimental results. The normalized transverse emittance was calculated as 1.4 μm. By contrast, in the case without the density bump, the first self-injected electrons in the second bucket could be accelerated but rapidly entered into the deceleration region owing to the phase slippage, and the decelerated electrons could not be seeded into the first bucket for re-acceleration.

In conclusion, we have experimentally realized a cascaded LWFA scheme using a controllable self-injection and acceleration method in the second bucket of the laser-driven wakefield. A steep density bump is constructed between the high-density injector and the low-density accelerator to stop the re-injection and rapid dephasing. The enhanced acceleration in the bump region can thus produce a high-quality seed e beam in a quasi-phase-stable way via re-phasing [23,29] before being seeded into the first bucket of the second-segment plasma. Moreover, the seed e beam witnessed a segment of negative-slope wakefield in the downward density ramp where the energy chirp was reversed to the negative one. Therefore, the growth of the e beam's absolute energy spread could be significantly suppressed owing to the chirp compensation in the re-acceleration in the low-density accelerator. High-quality tunable e beams with energies in the range of 200–600 MeV, 0.4%–1% rms energy spread, 10–80 pC charge, and ~0.2 mrad rms divergence have been experimentally produced. The achieved 6D brightness $B_{6D,n}$ in the range of 10^{15}–10^{16} A/m^2/0.1% is very close to the typical brightness of e beams from state-of-the-art linac drivers [14]. 3D PIC simulations support this scheme for generating controllable high-quality e beams as well. It is anticipated that

these all-round high-quality e beams will lead to the realization of compact monoenergetic gamma-ray and intense coherent x-ray radiation sources [17,26,30–32].

---

[*] michaeljs_liu@siom.ac.cn
[†] ruxinli@mail.shcnc.ac.cn
[‡] zzxu@mail.shcnc.ac.cn
[1] T. Tajima and J. M. Dawson, Phys. Rev. Lett. **43**, 267 (1979).
[2] C. G. R. Geddes, Cs. Toth, J. van Tilborg, E. Esarey, C. B. Schroeder, D. Bruhwiler, C. Nieter, J. Cary, and W. P. Leemans, Nature (London) **431**, 538 (2004).
[3] S. P. D. Mangles et al., Nature (London) **431**, 535 (2004).
[4] J. Faure, Y. Glinec, A. Pukhov, S. Kiselev, S. Gordienko, E. Lefebvre, J.-P. Rousseau, F. Burgy, and V. Malka, Nature (London) **431**, 541 (2004).
[5] H. T. Kim, K. H. Pae, H. J. Cha, I. J. Kim, T. J. Yu, J. H. Sung, S. K. Lee, T. M. Jeong, and J. Lee, Phys. Rev. Lett. **111**, 165002 (2013).
[6] X. Wang et al., Nat. Commun. **4**, 1988 (2013).
[7] W. P. Leemans et al., Phys. Rev. Lett. **113**, 245002 (2014).
[8] C. Rechatin, J. Faure, A. Ben-Ismail, J. Lim, R. Fitour, A. Specka, H. Videau, A. Tafzi, F. Burgy, and V. Malka, Phys. Rev. Lett. **102**, 164801 (2009).
[9] M. Mirzaie et al., Sci. Rep. **5**, 14659 (2015).
[10] J. S. Liu et al., Phys. Rev. Lett. **107**, 035001 (2011).
[11] A. J. Gonsalves et al., Nat. Phys. **7**, 862 (2011).
[12] W. Wang et al., Appl. Phys. Lett. **103**, 243501 (2013).
[13] B. B. Pollock et al., Phys. Rev. Lett. **107**, 045001 (2011).
[14] S. Di Mitri and M. Cornacchia, Phys. Rep. **539**, 1 (2014).
[15] G. R. Plateau et al., Phys. Rev. Lett. **109**, 064802 (2012).
[16] R. Weingartner et al., Phys. Rev. ST Accel. Beams **15**, 111302 (2012).
[17] Z. Huang, Y. Ding, and C. B. Schroeder, Phys. Rev. Lett. **109**, 204801 (2012).
[18] Y. Xu et al., Opt. Laser Technol. **79**, 141 (2016).
[19] T. Bonnet, M. Comet, D. Denis-Petit, F. Gobet, F. Hannachi, M. Tarisien, M. Versteegen, and M. M. Aléonard, Rev. Sci. Instrum. **84**, 103510 (2013).
[20] W. Lu, M. Tzoufras, C. Joshi, F. S. Tsung, W. B. Mori, J. Vieira, R. A. Fonseca, and L. O. Silva, Phys. Rev. ST Accel. Beams **10**, 061301 (2007).
[21] W. Li et al., Appl. Phys. Lett. **104**, 093510 (2014).
[22] W. Rittershofer, C. B. Schroeder, E. Esarey, F. J. Grüner, and W. P. Leemans, Phys. Plasmas **17**, 063104 (2010).
[23] Z. Zhang et al., New J. Phys. **17**, 103011 (2015).
[24] A. Buck et al., Phys. Rev. Lett. **110**, 185006 (2013).
[25] O. Lundh et al., Nat. Phys. **7**, 219 (2011).
[26] K. T. Phuoc, S. Corde, C. Thaury, V. Malka, A. Tafzi, J. P. Goddet, R. C. Shah, S. Sebban, and A. Rousse, Nat. Photonics **6**, 308 (2012).
[27] A. Buck, M. Nicolai, K. Schmid, C. M. S. Sears, A. Sävert, J. M. Mikhailova, F. Krausz, M. C. Kaluza, and L. Veisz, Nat. Phys. **7**, 543 (2011).
[28] C. Nieter and J. R. Cary, J. Comput. Phys. **196**, 448 (2004).
[29] E. Guillaume et al., Phys. Rev. Lett. **115**, 155002 (2015).
[30] N. D. Powers et al., Nat. Photonics **8**, 28 (2013).
[31] C. Feng, D. Xiang, H. Deng, D. Huang, D. Wang, and Z. Zhao, Opt. Express **23**, 14993 (2015).
[32] K. Nakajima, Nat. Phys. **4**, 92 (2008).